Inhibition of CRISPR-Cas9 with Bacteriophage Proteins

Graphical Abstract
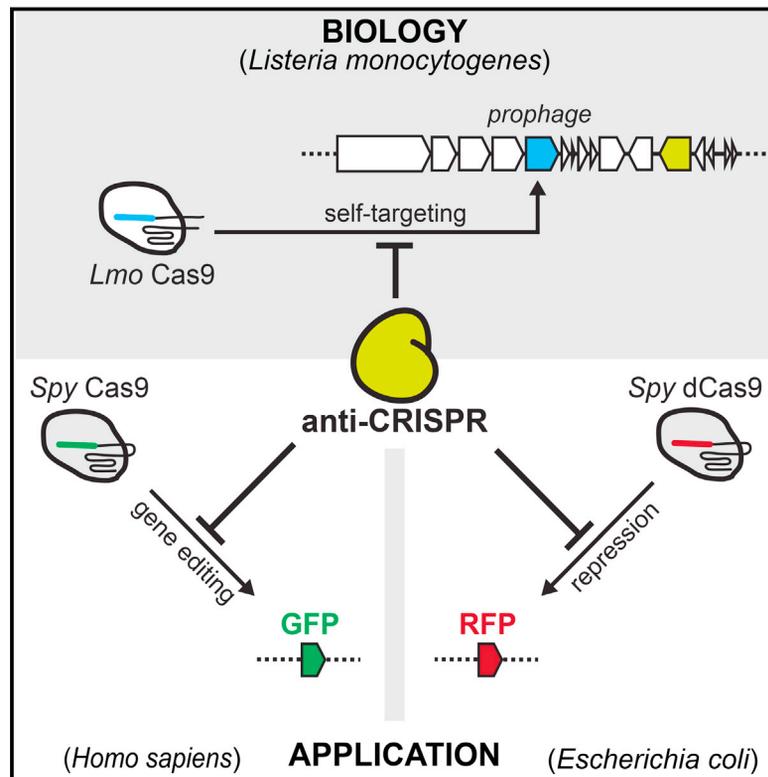
Authors

Benjamin J. Rauch, Melanie R. Silvis, Judd F. Hultquist, Christopher S. Waters, Michael J. McGregor, Nevan J. Krogan, Joseph Bondy-Denomy

Correspondence

joseph.bondy-denomy@ucsf.edu

In Brief

Four CRISPR-Cas9 inhibitor proteins encoded by *Listeria monocytogenes* prophages prevent Cas9 binding and gene editing in bacteria and human cells, including currently the most widely used Cas9 from *Streptococcus pyogenes*.

Highlights

- Bacteriophage anti-CRISPR proteins inactivate *Listeria monocytogenes* CRISPR-Cas9

- Half of *L. monocytogenes* isolates possess inhibited CRISPR-Cas9 systems

- AcrIIA2 and AcrIIA4 prevent target binding by dCas9 in bacteria

- AcrIIA2 and AcrIIA4 inhibit Cas9-mediated gene editing in human cells

CellPress

Article

Inhibition of CRISPR-Cas9 with Bacteriophage Proteins

Benjamin J. Rauch,[1,2] Melanie R. Silvis,[1,3] Judd F. Hultquist,[2,4,5] Christopher S. Waters,[1,2,3] Michael J. McGregor,[2,4,5] Nevan J. Krogan,[2,4,5] and Joseph Bondy-Denomy[1,2,6,*]

[1]Department of Microbiology and Immunology, University of California, San Francisco, San Francisco, CA 94158, USA
[2]Quantitative Biosciences Institute, QBI, University of California, San Francisco, San Francisco, CA 94158, USA
[3]Tetrad Graduate Program, University of California, San Francisco, San Francisco, CA 94158, USA
[4]Department of Cellular and Molecular Pharmacology, University of California, San Francisco, San Francisco, CA 94158, USA
[5]J. David Gladstone Institutes, San Francisco, CA 94158, USA
[6]Lead Contact
*Correspondence: joseph.bondy-denomy@ucsf.edu
http://dx.doi.org/10.1016/j.cell.2016.12.009

SUMMARY

Bacterial CRISPR-Cas systems utilize sequence-specific RNA-guided nucleases to defend against bacteriophage infection. As a countermeasure, numerous phages are known that produce proteins to block the function of class 1 CRISPR-Cas systems. However, currently no proteins are known to inhibit the widely used class 2 CRISPR-Cas9 system. To find these inhibitors, we searched *cas9*-containing bacterial genomes for the co-existence of a CRISPR spacer and its target, a potential indicator for CRISPR inhibition. This analysis led to the discovery of four unique type II-A CRISPR-Cas9 inhibitor proteins encoded by *Listeria monocytogenes* prophages. More than half of *L. monocytogenes* strains with *cas9* contain at least one prophage-encoded inhibitor, suggesting widespread CRISPR-Cas9 inactivation. Two of these inhibitors also blocked the widely used *Streptococcus pyogenes* Cas9 when assayed in *Escherichia coli* and human cells. These natural Cas9-specific "anti-CRISPRs" present tools that can be used to regulate the genome engineering activities of CRISPR-Cas9.

INTRODUCTION

The ability to prevent attack from viruses is a hallmark of cellular life. Bacteria employ multiple mechanisms to resist infection by bacterial viruses (phages), including restriction enzymes and CRISPR-Cas systems (Labrie et al., 2010). CRISPR arrays consist of the DNA remnants of previous phage encounters (spacers), located between clustered regularly interspaced short palindromic repeats (Mojica et al., 2005). These spacers are transcribed to generate CRISPR RNAs (crRNAs) that direct the binding and cleavage of specific nucleic acid targets (Brouns et al., 2008; Garneau et al., 2010). The CRISPR-associated (cas) genes required for immune function are often found adjacent to the CRISPR array (Marraffini, 2015; Wright et al., 2016). Cas proteins perform many functions, including destroying foreign genomes (Garneau et al., 2010), mediating the acquisition of foreign sequences into the CRISPR array (Nuñez et al., 2014; Yosef et al., 2012), and facilitating the production of mature CRISPR RNAs (crRNAs) (Deltcheva et al., 2011; Haurwitz et al., 2010).

CRISPR-Cas adaptive immune systems are both common and diverse in the bacterial world. Two distinct classes, encompassing six CRISPR types (I–VI) have been identified across bacterial genomes (Abudayyeh et al., 2016; Makarova et al., 2015), each with the ability to cleave target DNA or RNA molecules with sequence specificity directed by the RNA guide. The facile programmability of CRISPR-Cas systems has been widely exploited, opening the door to an array of novel genetic technologies, most prominently gene editing in animal cells (Barrangou and Doudna, 2016). Most technologies are based on Cas9 (class 2, type II-A) from *Streptococcus pyogenes* (Spy), together with an engineered single guide RNA (sgRNA) because of the simplicity of the system (Jinek et al., 2012). Gene editing in animal cells has been successful with Spy Cas9 (Cong et al., 2013; Mali et al., 2013), Cas9 orthologs within the II-A subtype (Ran et al., 2015), and new class 2 single protein effectors such as Cpf1 (type V) (Zetsche et al., 2015). Applications are also being developed through the characterization of type VI CRISPR-Cas systems, represented by C2c2, which naturally cleave RNA (Abudayyeh et al., 2016; East-Seletsky et al., 2016). In contrast, the complex class 1 CRISPR-Cas systems (type I, type III, and type IV), consisting of RNA-guided multi-protein complexes and thus have been overlooked for most genomic applications. These systems are, however, the most common in nature, comprising ~75% of all bacterial CRISPR-Cas systems and nearly all systems in archaea (Makarova et al., 2015).

In response to the bacterial war on phage infection, phages, in turn, often encode inhibitors of bacterial immune systems that enhance their ability to either lyse their host bacterium or integrate into its genome (Samson et al., 2013). The first examples of phage-encoded "anti-CRISPR" proteins came for the class 1 type I-F and I-E systems in *Pseudomonas aeruginosa* (Bondy-Denomy et al., 2013; Pawluk et al., 2014). Remarkably, ten type I-F anti-CRISPR and four type I-E anti-CRISPR genes have been discovered to date (Pawluk et al., 2016), all of which encode distinct, small proteins (50–150 amino acids), previously of unknown function. Our biochemical investigation of four I-F

Cell
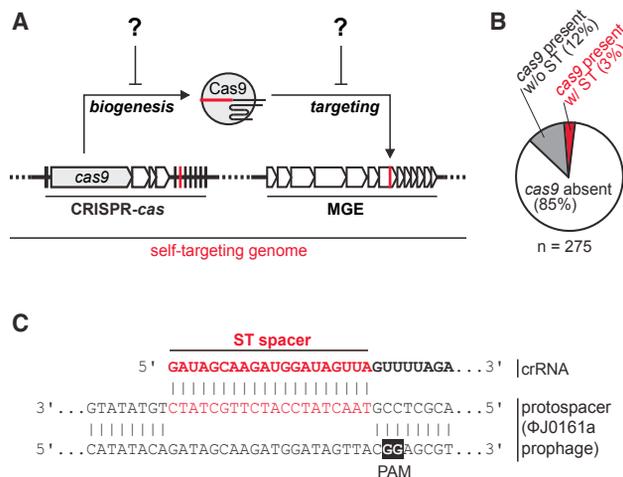
Figure 1. A Survey for CRISPR-Cas9 Genomic Self-Targeting in *Listeria monocytogenes*

(A) A schematic depicting the principle of genomic self-targeting, where a mobile genetic element (MGE) possesses a target sequence for a spacer in a CRISPR array in the same genome. CRISPR-Cas9 function in this "self-targeting genome" is presumably inactive for continued cell viability.

(B) The abundance of genomes with (red) and without (gray) *cas9*-linked self-targeting (ST), in *L. monocytogenes* genomes. See Table S1 for a list of self-targeting strains.

(C) An example of an ST event, where spacer 16 in the type II-A CRISPR array of strain J0161 has a perfect PAM and protospacer match with a resident prophage (φJ0161a). See Figure S1B for the entire CRISPR array.

anti-CRISPR proteins revealed that they directly interact with different Cas proteins in the multi-protein CRISPR-Cas complex to prevent either the recognition or cleavage of target DNA (Bondy-Denomy et al., 2015). Anti-CRISPR proteins have distinct sequences (Bondy-Denomy et al., 2013), structures (Maxwell et al., 2016; Wang et al., 2016), and modes of action (Bondy-Denomy et al., 2015). These findings support the independent evolution of CRISPR-Cas inhibitors and suggests that many more are yet to be discovered. Indeed, a recent investigation exploited the conservation of signature anti-CRISPR-associated (aca) gene with a predicted helix-turn-helix (HTH) motif to identify anti-CRISPRs across proteobacteria, broadly spanning the type I-F CRISPR-Cas phylogeny (Pawluk et al., 2016).

Although anti-CRISPRs are both prevalent and diverse within proteobacteria, it is presently unknown whether anti-CRISPR proteins occur in other bacterial phyla. Likewise, it is also unclear if anti-CRISPRs exist for systems other than types I-E and I-F. In *P. aeruginosa*, type I anti-CRISPRs are expressed from integrated phage genomes (prophages) and cause the constitutive inactivation of the host CRISPR-Cas system (Bondy-Denomy et al., 2013). In such cases, the prophage can possess a DNA target with perfect identity to a CRISPR spacer in the same cell, as the CRISPR-Cas system is inactivated. The genomic co-occurrence of a spacer and its target DNA with a perfect match is called "self-targeting" (Figure 1A). Bacteria with self-targeting require CRISPR-Cas inactivation for survival; in the absence of anti-CRISPR genes, the host genome will be cleaved in the act of targeting the prophage (Bondy-Denomy et al., 2013; Edgar and

Qimron, 2010). Expression of an anti-CRISPR, therefore, neutralizes this risk. We surmised that genomes possessing a CRISPR system with apparent self-targeting would be candidates for the identification of new CRISPR-Cas inhibitors. Here, we describe the identification of four previously unknown phage-encoded CRISPR-Cas9 inhibitors in *Listeria monocytogenes* using a bioinformatics approach to identify incidents of self-targeting. We also demonstrate that two of these inhibitors can block the activity of *S. pyogenes* Cas9 in bacterial and human cells.

RESULTS

CRISPR-Cas9 in *Listeria monocytogenes* Targets Foreign DNA

Listeria monocytogenes is a facultative intracellular food-borne pathogen with a well-characterized phage population. Many *L. monocytogenes* isolates have type II-A CRISPR-Cas systems (Sesto et al., 2014) and their CRISPR spacers possess identity to many virulent, temperate, and integrated phages (Di et al., 2014; Sesto et al., 2014). However, there is no experimental evidence of canonical CRISPR-Cas function. We analyzed 275 genomes of *L. monocytogenes* and identified type II-A CRISPR-Cas9 systems (Lmo Cas9) in 15% (n = 41) of them (Figure 1B). Interestingly, we found eight genomes (3% of the total), with examples of self-targeting (ST) (Figures 1B and 1C; Table S1), although the CRISPR-Cas9 system is anticipated to be functional as all requisite genes are present with no obvious mutations (Figure S1A). Many self-targeted protospacers were found in prophages, and thus we predicted that these prophages encode inhibitors of CRISPR-Cas9 that allow the stable co-existence of a spacer-protospacer pair.

To test whether inhibitors were encoded by the prophages of *L. monocytogenes*, we first established the functionality of CRISPR-Cas9 in an *L. monocytogenes* strain (10403s) that does not exhibit self-targeting. To test the activity of this system we designed a plasmid (pT) possessing a targeted protospacer (i.e., a sequence that is complementary to a natural spacer in the CRISPR array) along with a cognate protospacer adjacent motif (PAM), a three base motif that is necessary for Cas9 binding (Figure 2A). We measured the transformation efficiency of 10403s with either pT or a control plasmid possessing a non-targeted sequence with an identical plasmid backbone (pNT). Transformation with pT yielded miniscule colonies relative to pNT (Figure 2B, leftmost panel), although the number of colonies that emerged upon prolonged incubation were the same (see Discussion for further analysis). To determine whether the 10403s prophage (φ10403s) was inhibiting CRISPR-Cas9 function in any way, a prophage-cured version of this strain (φcure) was tested, yielding the same tiny colonies (Figure 2B). The φcure strain was used for all subsequent experiments because it was indistinguishable from wt10403s in this assay. To confirm that the observed transformation inhibition was the result of CRISPR-Cas9 interference, we constructed a *cas9*-deletion strain. Transformation of this strain with pT and pNT produced colonies of indistinguishable size (Figure 2B). However, adding back *cas9* to the *L. monocytogenes* chromosome under a constitutively active promoter completely prevented transformation with pT (Figure 2B, rightmost panel).
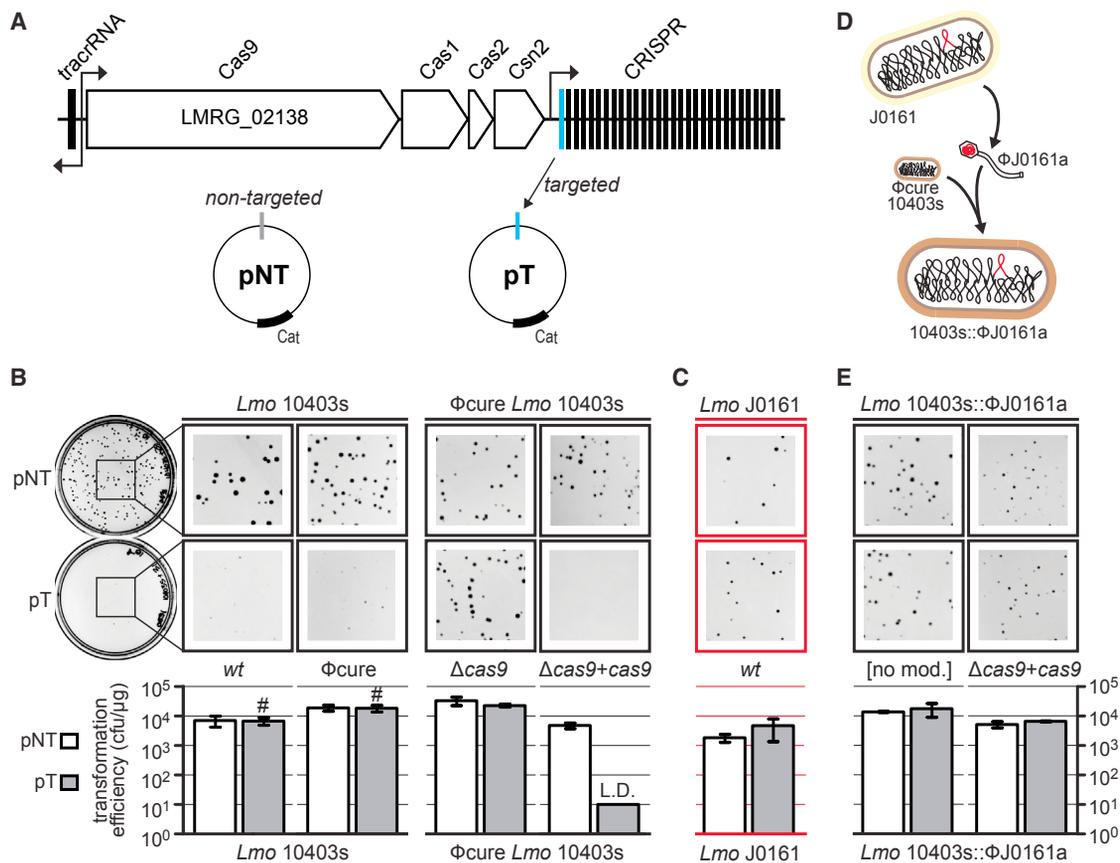
Figure 2. A Prophage from *L. monocytogenes* J0161 Inhibits CRISPR-Cas9 Function

(A) The type II-A CRISPR-Cas locus in *L. monocytogenes* 10403s. Four *cas* genes and the upstream tracrRNA are indicated, along with a CRISPR array containing 30 spacers. The predicted direction of transcription is indicated with black arrows. Subsequent experiments utilize a non-targeted plasmid (pNT) and a targeted plasmid (pT) that has a protospacer matching spacer 1 in this strain.

(B) Representative pictures of colonies of *Lmo* 10403s wild-type (wt), prophage-cured (ϕcure), *cas9*-deletion strain (Δ*cas9*), and a *cas9* overexpression strain (Δ*cas9* + *cas9*) after being transformed with pT or pNT plasmids. Bar graphs below the plates show the calculated transformation efficiency (colony forming units per μg of plasmid). Data are represented as the mean of three biological replicates ± SD. L.D., limit of detection; transformants with small colonies denoted with #.

(C) Plasmid-targeting assay with wild-type J0161 (contains the ϕJ0161a prophage; experiment conducted as in [B], except with pT$_{J0161}$ as the targeted plasmid) is shown in red to denote self-targeting (as in Figure 1).

(D) A schematic demonstrating the construction of a 10403s strain containing the prophage ϕJ0161a (10403s::ϕJ0161a). See the STAR Methods for details.

(E) Plasmid-targeting assay with 10403s lysogenized with the ϕJ0161a prophage (10403s::ϕJ0161a) with endogenous (no mod) or overexpressed *cas9* (Δ*cas9* + *cas9*; experiment conducted as in [B]).

Together, these experiments demonstrate that Cas9 is functional in *L. monocytogenes* 10403s at both endogenous and overexpressed levels and limits transformation with a plasmid bearing a protospacer.

Resident Prophages Inactivate CRISPR-Cas9 in *L. monocytogenes*

To determine whether CRISPR-Cas9 may be disabled in a strain with self-targeting spacers, we examined immunity function in *L. monocytogenes* strain J0161, whose spacer 16 perfectly matches a prophage (ϕJ0161a) in the same genome (Figure 1C). We could not detect any clearly deleterious CRISPR-Cas mutations in the CRISPR repeat, PAM, tracrRNA, Cas9, and the associated promoters of strain J0161 (Figures S1B–S1F and S2), suggesting that this self-targeting scenario was the result of inhibition and not loss of function. Because the type

II-A CRISPR array of J0161 is distinct from that of 10403s, a J0161-specific targeted plasmid (pT$_{J0161}$) was used to test the function CRISPR-Cas9 in J0161. Consistent with the inactivation implied by self-targeting, there were no significant differences in transformation efficiency or colony size to distinguish pT$_{J0161}$ from pNT (Figure 2C). Thus, we reasoned that the J0161 genome may encode Cas9 inhibitors.

In search of the genetic basis for CRISPR-Cas9 inactivation in J0161, we focused on the prophage ϕJ0161a as a likely source of an inhibitor gene because it contained the self-targeted sequence in this strain. To determine whether ϕJ0161a contained an inhibitor, the prophage-cured strain of 10403s was lysogenized with ϕJ0161a and assayed for CRISPR-Cas9 functionality by plasmid transformation (Figure 2D). The acquisition of ϕJ0161a was sufficient to inactivate CRISPR-Cas9 function (Figure 2E, left panels), suggesting that this prophage encodes an

Cell
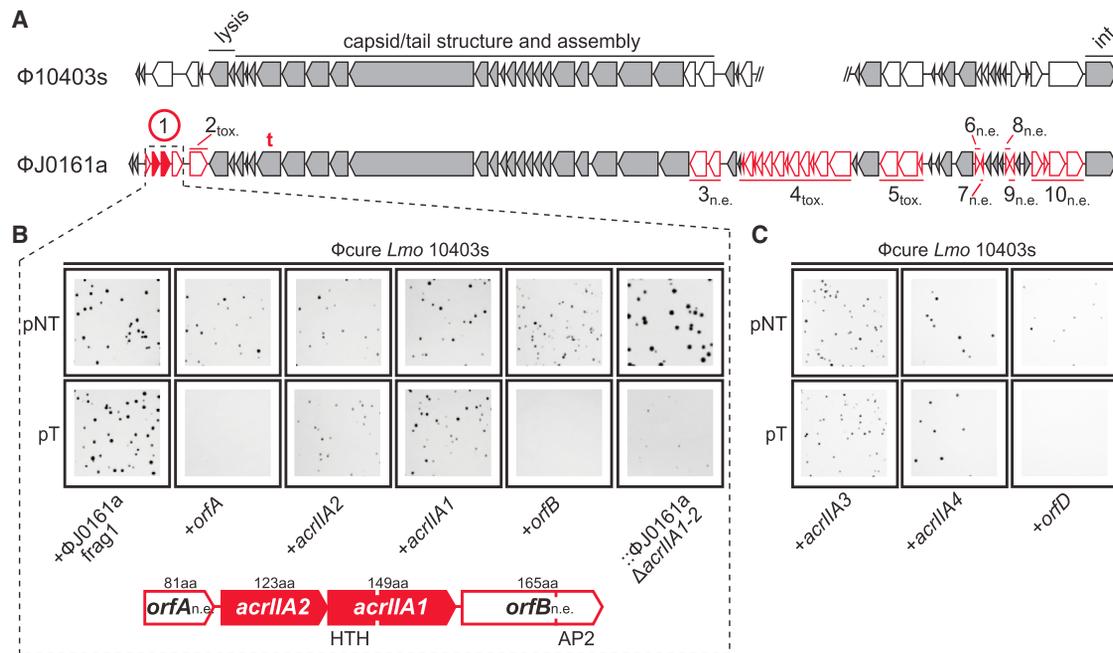
Figure 3. Identification of Four Distinct Anti-CRISPR Proteins

(A) Comparison of the open reading frames from two similar prophages from *L. monocytogenes* 10403s and J0161. Unique genes (red) comprising ten fragments of ϕJ0161 were tested for CRISPR-Cas9 inhibition in 10403s. n.e., no effect on CRISPR-Cas9 activity; tox., fragment toxic when expressed; t., location of self-targeted protospacer. The encircled fragment exhibited anti-CRISPR activity with two genes (*acrAII1*, *acrAII2*) independently capable of inhibiting CRISPR-Cas activity. Conserved (gray) genes were not tested. For reference, phage genes involved in cell lysis, capsid assembly, and host integration (int.) are labeled.

(B) Representative colony pictures of Lmo 10403s ϕcure strains constitutively expressing "fragment 1" (as shown in A) or the indicated individual genes from ϕJ0161a transformed with pNT or pT. The rightmost panels show a 10403s lysogen of ϕJ0161a with CRISPR-Cas9 inhibitor genes deleted (::ϕJ0161aΔ*acrIIA1-2*). See Figure S2 for data from the other ϕJ0161a fragments and Figures S2 and S3 for full plates.

(C) Representative colony pictures of Lmo 10403s ϕcure strains constitutively expressing *acrIIA3*, *acrIIA4*, or *orfD* transformed with pNT or pT.

inhibitor of CRISPR-Cas9. The ϕJ0161a prophage also inactivated plasmid targeting in a strain constitutively expressing *cas9*, suggesting that the inhibitory mechanism does not operate by disrupting natural regulation of the *cas9* promoter (Figure 2E, right panels).

Given that the ϕJ0161a prophage inhibited CRISPR-Cas9 function in 10403s and the endogenous ϕ10403s prophage did not, we compared the genomes of these two closely related phages to identify the regions of difference (Figure 3A). In addition to sharing 39 core phage genes with >40% protein sequence identity, ten non-overlapping unique clusters of genes were identified (cluster boundaries were chosen based on predicted operon structure, with 1–12 genes per cluster). Each cluster was cloned and integrated into the genome of prophage-cured 10403s and assayed for CRISPR-Cas9 function. Of the ten fragments, seven were successfully introduced into *L. monocytogenes*, while three fragments could not be inserted in the *L. monocytogenes* genome and were presumably toxic in isolation. Plasmid transformation assays revealed that ϕJ0161a fragment 1 was the only fragment capable of inhibiting CRISPR-Cas9, indicating that this fragment encoded at least one CRISPR-Cas9 inhibitor (Figure 3B). Expressing the individual genes from this four-gene fragment led to the conclusive identification of two anti-CRISPR genes, LMOG_03146 and LMOG_03147 (herein referred to as *acrIIA1* and *acrIIA2*, respectively) while LMOG_03145 and LMOG_03148 (*orfB* and *orfA*,

respectively) had no anti-CRISPR activity (Figure 3B). Deletion of both *acrIIA1* and *acrIIA2* from a 10403s::ϕJ0161a lysogen restored CRISPR-Cas9 function, confirming that these are the only anti-CRISPR genes in ϕJ0161a (Figure 3B, rightmost panels).

Anti-CRISPR Genes Are Widespread in *L. monocytogenes* Prophages

To identify additional type II-A anti-CRISPRs, we examined the genomic position analogous to that of *acrIIA1* and *acrIIA2* in related *L. monocytogenes* prophages. A recurring anti-CRISPR (*acr*) locus containing *acrIIA1* within a small operon (two to five genes) of highly conserved gene order was identified between the "left" integration site and the genes involved in cell lysis (Figure 4A). We identified five additional protein families conserved within *acr* loci. To test these families for anti-CRISPR function, we cloned and integrated representatives into the 10403s genome and assayed for transformation efficiency of pT and pNT. Two new genes were identified that were capable of CRISPR inactivation (*acrIIA3* and *acrIIA4*), while the remaining three (*orfC*, *orfD*, *orfE*) were not (Figures 3C and S3).

To determine whether CRISPR-Cas9 inactivation in *L. monocytogenes* is pervasive, we next analyzed the conservation pattern for each anti-CRISPR. Although each *acrIIA* gene was sufficient to inactivate CRISPR-Cas9 in isolation, we observed a common presence of *acrIIA1* in most *acr* loci. Nearly
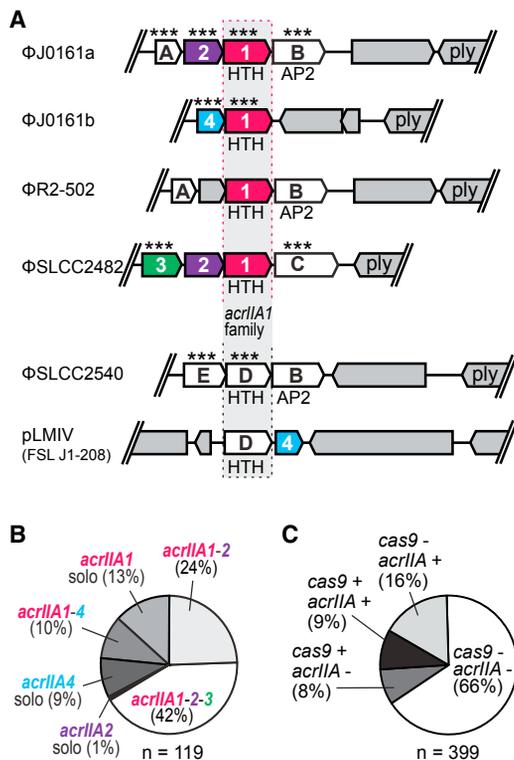
Figure 4. Genomic Organization and Prevalence of *acrIIA* Genes

(A) The genomic context of *acrIIA1* (1) and its homolog from *L. monocytogenes* (*orfD*) are depicted to scale as cartoons with *acrIIA1* homologs in vertical alignment. Typically, *acrIIA* genes are encoded within prophages adjacent to or near the phage lysin (*ply*) gene. Genomic neighbors of *acrIIA1* and *orfD* (*acrIIA1-4, orfA-E*) are shown. Individual genes (***) were assayed for CRISPR-Cas9 inhibition in *L. monocytogenes* 10403s (see Figures 3 and S3). Helix-turn-helix (HTH) and AP2 DNA binding motifs were detected in some proteins using hidden Markov model (HMM) prediction software (Söding et al., 2005).

(B) Pie-graph representation of the frequency of each *acrIIA* gene co-occurrences

(C) Pie-graph representation of the prevalence of *acrIIA* and *cas9* genes in the *L. monocytogenes* pan-genome.

See Table S1 for relevant accession numbers.

Figure 5. Phylogenetic Analysis of AcrIIA1-4 Homologs

An unrooted phylogenetic reconstruction of full-length protein sequences identified following an iterative psi-BLASTp search to query all non-redundant protein sequences within GenBank for (A) AcrIIA1. BLASTp was used to identify sequences for similar phylogenetic reconstructions of (B) AcrIIA2, (C) AcrIIA3, and (D) AcrIIA4 (see the STAR Methods). Selected bootstrapping support values are denoted with filled ovals (≥90%), open rectangles (≥70%) or dashed lines (<70%). The sequence family that is boxed-in represents the family that was tested for anti-CRISPR function. Other homologs reflect distinct sub-families present in the genomes described under the tree.

all instances (88%) of *acrIIA2-4* were found upstream of the helix-turn-helix (HTH) motif-containing *acrIIA1*, suggesting that this gene may be a marker for *acr* loci (Figures 4A and 4B). The most common scenario in 119 *acr* loci was either *acrIIA1-2* or *acrIIA1-2-3*, together representing 66% of *acr* loci (Figure 4B). In total, *acrIIA* genes were identified in 25% of *L. monocytogenes* genomes, with 53% of *cas9*-containing *L. monocytogenes* strains possessing at least one anti-CRISPR in the same genome (Figure 4C). Many instances of *L. monocytogenes* genomes possessing multiple *acrIIA*-encoding prophages were also identified (Table S1). Furthermore, at least one *acrIIA* gene was found in the genomes of all eight instances of self-targeting that were initially identified (Figure 1B; Table S1), explaining how these scenarios are stable. Together, these data suggest widespread prophage-mediated inactivation of CRISPR-Cas9 in *L. monocytogenes*.

Previous HTH-containing anti-CRISPR-associated (*aca*) genes were used as markers to identify novel type I anti-CRISPR genes (Pawluk et al., 2016), although the *aca* genes did not have anti-CRISPR activity themselves. We hypothesized that *acrIIA1* could fulfill the role of such a marker. A comprehensive phylogenetic analysis of *acrIIA1* revealed that homologs were conserved widely across Firmicutes, in both mobile elements and core genomes (Figure 5A). A family of distantly related *acrIIA1* homologs was identified in *Listeria* genomes, as exemplified by the *orfD* gene, which had been independently identified as an *acr* locus member that also occurs upstream of *acrIIA4* homologs in contexts outside of prophages (Figure 4A; Table S1). While *orfD* lacked anti-CRISPR activity in a functional assay (Figure 3B), its co-occurrence with a bona fide *acr* gene suggests that the broad *acrIIA1/orfD* superfamily could be used as a marker to identify new *acr* genes. Future work will be necessary to determine whether the HTH-containing genes in these systems serve as effective markers for novel anti-CRISPR discovery.

To determine the homology landscape of *acrIIA2-4*, additional phylogenetic analyses were performed. Unlike *acrIIA1*, which was widespread across Firmicutes core genomes, the other three *acr* genes were mostly restricted to prophages in *Listeria*. Three distinct sequence families of *acrIIA2* were identified, all restricted to *Listeria* siphophages (a family of long-tailed, non-contractile phages) (Figure 5B), while two *acrIIA3* families were observed in the genomes of siphophages infecting *Listeria* and *Streptococcus* (Figure 5C). Lastly, *acrIIA4* was observed in two
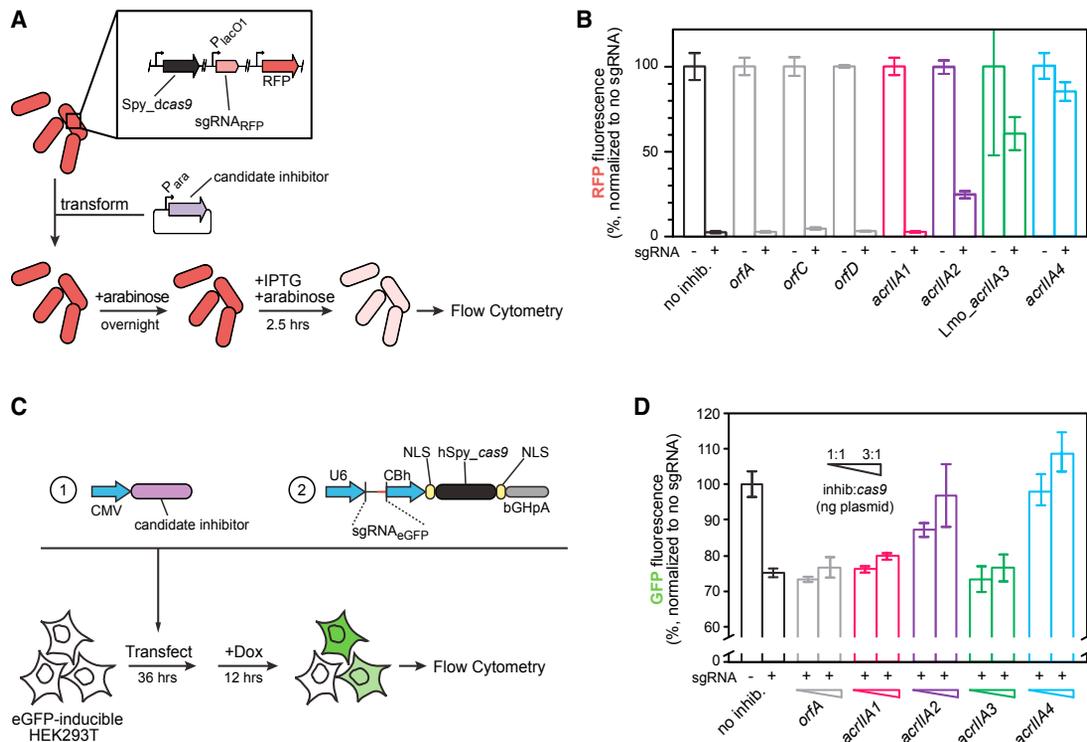
Cell

Figure 6. Inhibition of *Streptococcus pyogenes* dCas9 and Cas9

(A) A schematic outlining the experimental setup, where single-cell fluorescence of *E. coli* BW25113 expressing *Streptococcus pyogenes* (Spy) dCas9 and a sgRNA targeted toward a chromosomal red fluorescent protein (RFP) gene was measured by flow cytometry.

(B) Candidate (*orf*) and validated (*acr*) *acrIIA* genes were tested for their ability to inhibit dCas9-based gene repression. Measurements taken reflect the median RFP fluorescence value of a single cell in a unimodal population normalized for each candidate gene to a sgRNA-free control. Error bars represent the mean ± SD of at least three biological replicates. See Figures 3 and S3 for gene-identification information. See Figure S4 for raw flow cytometry data.

(C) A schematic outlining the experimental setup, where HEK293T cells with a chromosomally integrated, doxycycline-inducible eGFP cassette were transfected with a plasmid encoding a single transcript tracrRNA/eGFP-targeting sgRNA and NLS-SpyCas9 alongside expression constructs encoding one of five codon-optimized phage genes at different ratios. The percent of eGFP-positive cells was measured 12 hr after induction by flow cytometry.

(D) Candidate (*orf*) and validated (*acr*) *acrIIA* genes were tested for their ability to inhibit dCas9-based gene editing. An increasing amount of inhibitor plasmid (in ng) was added from left to right, at a ratio to the Cas9/sgRNA plasmid of 1:1 and 3:1. Data were normalized to transfection with no phage ORF as the baseline. Average percent of eGFP-positive cells is depicted ± SD across biological triplicates. See Figure S5 for raw flow cytometry data.

distinct sequence families, one in *Listeria* siphophages and plasmids and the other in a group of obligate virulent myophages (long contractile-tailed phages) (Figure 5D). While *acrIIA2* and *acrIIA3* were nearly always found with *acrIIA1*, *acrIIA4* often occurred in the absence of *acrIIA1* homologs in phages and mobile elements of *Listeria*. For example, the family of *acrIIA4* in virulent phages are distinct from the other family of *acrIIA4* homologs in that they have an ~70 amino acid C-terminal extension in the predicted protein and do not occur with the HTH-containing genes *acrIIA1* or *orfD*, suggesting potential mechanistic and evolutionary distinctions between these *acrIIA4* families. Together, these analyses reveal ample sequence space for surveying homologous *acr* genes for specificity determinants and suggest an active arms race between *cas9* and mobile elements in *L. monocytogenes*.

AcrIIA2 and AcrIIA4 Inhibit *S. pyogenes* Cas9

To determine the versatility of the Lmo Cas9 AcrIIA proteins, we asked whether these inhibitors were functional on the related

Cas9 protein from *S. pyogenes* (Spy, 53% identical to Lmo Cas9). This ortholog has been used widely for biotechnological applications as an RNA-guided nuclease (Barrangou and Doudna, 2016), as well as for programmable gene repression by a catalytically deactivated mutant (dCas9) (Gilbert et al., 2013; Qi et al., 2013). Using an *E. coli* strain that carries Spy dCas9, we tested whether AcrIIA proteins block dCas9 from interfering with transcription of a chromosomal RFP reporter gene (Figure 6A). In a genetic background lacking inhibitors, the presence of an sgRNA and dCas9 reduced RFP fluorescence ~40-fold (2.6% relative to that of a strain with no sgRNA). *acrIIA1* had no impact on dCas9-mediated transcriptional repression, nor did *orfA*, *orfC*, or *orfD*, which were employed as negative controls. *acrIIA2* partially blocked dCas9 function, with fluorescence reduced only 4-fold (25% relative to the no guide control), while *acrIIA4* nearly completely blocked dCas9, with fluorescence at 85% of the no guide control (Figure 6B). We could not obtain meaningful data from *acrIIA3* because the protein was toxic to *E. coli*. This lowered the recorded cell count during flow cytometry

Cell

(see Figure S4A) and lead to large variability in the fluorescence measurements. A homolog of *acrIIA3* from *S. pyogenes* (accession number NCBI: AND04610.1) with 45% sequence identity to Lmo_*acrIIA3* was tested, but also resulted in impaired growth of *E. coli* (Figures S4B and S4C). The mechanism of *acrIIA3* toxicity in *E. coli* remains to be determined. We conclude that the *acrIIA2* and *acrIIA4* inhibit Spy dCas9 in *E. coli* to different degrees.

Given the common application of Spy Cas9 in eukaryotic cells, we next tested the AcrIIA proteins for their ability to block gene editing in human cells. HEK293T cells with an inducible, chromosomally integrated eGFP reporter gene were transiently transfected with a plasmid expressing both Spy Cas9 and an sgRNA targeting eGFP in the presence or absence of vectors expressing human codon optimized *acrIIA* genes. After allowing gene editing to proceed for 36 hr, eGFP was induced for 12 hr, and cellular fluorescence was then measured by flow cytometry (Figure 6C). In the presence of Cas9 and the eGFP sgRNA, gene editing resulted in a 25% decrease in the number of GFP-positive cells, while co-expression with *acrIIA2* or *acrIIA4* prevented Cas9-based gene editing (Figure S5; Figure 6D). We additionally tested the *S. pyogenes* homolog of *acrIIA3* (Spy_*acrIIA3*), which was not toxic in human cells, but it had no impact on Cas9 function in this assay. *acrIIA1* was non-functional in human cells, as was the negative control, *orfA*. Taken together with dCas9 experiments in *E. coli*, these data demonstrate the utility of the AcrIIA2 and AcrIIA4 proteins to inhibit the function of an orthologous Cas9 in heterologous hosts. These reagents, therefore, represent new tools in the CRISPR-Cas9 genome engineering toolkit.

DISCUSSION

Phage-encoded inhibitors of bacterial immune systems emerge due to the strong selective pressures in the evolutionary arms race between these two entities (Samson et al., 2013). The first identification of phage encoded anti-CRISPRs in type I CRISPR-Cas systems hinted that more CRISPR-Cas inhibitors existed, but methods were lacking for their discovery. Here, we present a bioinformatics strategy that uses "self-targeting" as a genomic marker for CRISPR-Cas inhibitor genes (Figure 1A). This approach led to the identification of four different type II-A CRISPR-Cas9 inhibitors (Figures 3 and 4A), which are collectively present in half of all Cas9-encoding *L. monocytogenes* genomes, including all genomes with self-targeting (Figure 4C). We anticipate that this approach will be helpful for identifying *acr* genes in other CRISPR-Cas systems, although a distinct mechanism for tolerance of self-targeting has been described for type III systems (Goldberg et al., 2014; Samai et al., 2015).

To facilitate the identification of AcrIIA proteins, we first demonstrate a functional CRISPR-Cas9 system in *L. monocytogenes* (Figure 2B). Previous studies of CRISPR-Cas in this organism have focused on the type I-B system and an associated orphan CRISPR array lacking *cas* genes (Mandin et al., 2007; Sesto et al., 2014). Although no canonical CRISPR-Cas function had been established for either system previously, the orphan array was shown to be processed by a host ribonuclease to generate non-coding RNAs (Mandin et al., 2007; Sesto et al., 2014). To observe function for the type II-A CRISPR-Cas system, we used a transformation efficiency assay, showing that CRISPR-

Cas9 function in strain 10403s is able to limit transformation of a plasmid in a sequence-specific manner (Figures 2A and 2B). Given the small colony phenotype observed during transformation of 10403s with the targeted plasmid (pT), we suspect that endogenous levels of *cas9* expression are not sufficient to totally clear the plasmid. Either a small fraction of cells retain the plasmid, or alternatively, cells temporarily possess the plasmid at a reduced copy number, resulting in the small colony phenotype. Consistent with low endogenous expression of *cas9* leading to either form of incomplete plasmid clearance, increased expression of *cas9* resulted in an elimination of detectable transformants in this assay (Figure 2B).

Among the strains with self-targeting, we selected J0161 for further analysis. Using the transformation efficiency assay, we observed no plasmid targeting in this strain (Figure 2C), an observation consistent with the presence of an inhibitor. Indeed, the immune system was inactivated when the ϕJ0161a prophage was transferred to the CRISPR-Cas9-active strain 10403s (Figure 2D). Furthermore, we observed that ϕJ0161a can inactivate CRISPR-Cas9 function in a strain that overexpresses Cas9 (Figure 2E). Mechanistically, this demonstrates that inhibitors are unlikely to function by disrupting the transcriptional regulation of Cas9 and are sufficiently expressed from the integrated prophage to cope with enhanced Cas9 levels.

To identify candidate anti-CRISPR genes, related prophages from CRISPR-active and inactive strains were compared, and a process-of-elimination cloning approach was taken (Figure 3A). Two isolated *acr* genes (*acrIIA1* and *acrIIA2*) were first identified in ϕJ0161a (Figure 3B). In searching for more anti-CRISPRs, we find that conserved genomic positioning in related phages is a good proxy for identifying distinct type II-A Cas9 inhibitor proteins, despite a lack of sequence conservation between the proteins themselves (Figure 4A). This has been observed previously in studies of type I-F and I-E anti-CRISPRs (Bondy-Denomy et al., 2013; Pawluk et al., 2014). In *L. monocytogenes*, the high prevalence of Cas9 inhibitors in prophages suggests the widespread inactivation of CRISPR-Cas9 function (Figure 4C). At present, we do not understand whether there is a mechanistic link to explain the common co-occurrence of *acrIIA1* with other anti-CRISPRs (Figures 4A and 4B). Although this gene is sufficient to inactivate CRISPR-Cas9 function in a plasmid challenge assay, we speculate that it could act as a co-factor or regulator of other *acrIIA* genes during infection or lysogeny, thus explaining the genomic associations observed. Future work will be necessary to understand whether AcrIIA1 is, in fact, a bi-functional protein in this regard and more broadly, whether its superfamily is a marker for *acr* genes.

Phylogenetic analyses demonstrate common occurrences of *acrIIA2-4* in mobile elements in *Listeria* mobile elements (Figure 5). Inhibiting the adaptive immune system likely aids horizontal gene transfer in this organism by blocking Cas9-based targeting and adaptation (Heler et al., 2015). In addition to the family of prophages where these *acrIIA* genes were first identified, homologs were also found in distant siphophages, myophages, and plasmids (Table S1). Most notably, the *acrIIA4* homologs encoded by virulent myophages did not have *acrIIA1* superfamily homologs in their vicinity. Furthermore, the presence of *acrIIA1* and *acrIIA3* homologs in genera outside of *Listeria*

Cell

demonstrates that CRISPR-Cas9 inactivation may be common-place in the Firmicutes.

Many potential mechanisms could explain CRISPR-Cas9 inactivation. In their native hosts, *L. monocytogenes,* we have defined anti-CRISPRs by their ability to inhibit Lmo Cas9-based targeting of a plasmid. Furthermore, by demonstrating the efficacy of *acrIIA2* and *acrIIA4* in heterologous hosts with engineered elements (i.e., *cas9* promoter, sgRNA design, and promoter) we conclude *acr*-mediated transcriptional repression of the CRISPR-Cas9 system is unlikely. Using the orthologous Spy Cas9, it is clear that AcrIIA2 and AcrIIA4 have broad specificity, given that Lmo Cas9 and Spy Cas9 only share 53% sequence identity. AcrIIA2 and AcrIIA4 likely target regions conserved between the two Cas9 proteins. Type I anti-CRISPRs function by binding directly to the Cas proteins required for target interference and preventing DNA binding or DNA cleavage (Bondy-Denomy et al., 2015). By extension, we expect a similar mechanism for AcrIIA2 and AcrIIA4, given their ability to function in heterologous hosts. Given the efficacy of AcrIIA4 in blocking dCas9-based function and, to a lesser extent, AcrIIA2 (Figure 6B), stable DNA-binding is likely inhibited, although whether this is through a direct interaction with Cas9 remains to be seen.

The identification and future mechanistic dissection of type II-A inhibitors will provide valuable new reagents for studying canonical CRISPR-Cas9 function in natural and engineered settings. The ability of AcrIIA proteins to block Spy Cas9 in *E. coli* and human cells suggests that these proteins can provide a post-translational "off-switch" for Cas9. This could add a layer of regulation on this powerful system that can be applied in eukaryotic systems to control genome engineering. This new addition to the CRISPR-Cas9 toolbox could enable new applications, such as specifically reversing the effects of dCas9 binding to a genomic locus, or limiting the amount of time that Cas9 is active in the nucleus to reduce off-target gene editing. It will be important to continue to exploit the abundant tools provided to us from the phage-bacteria arms race as we expand the CRISPR-Cas toolbox.

STAR★METHODS

Detailed methods are provided in the online version of this paper and include the following:

- KEY RESOURCES TABLE
- CONTACT FOR REAGENT AND RESOURCE SHARING
- EXPERIMENTAL MODEL AND SUBJECT DETAILS
  - Microbes
  - Cell lines
- METHOD DETAILS
  - Assay of CRISPR-Cas9 in L. monocytogenes
  - Bioinformatic analyses
  - Inhibition of Spy-CRISPRi in *E. coli*
  - Inhibition of Cas9 cleavage in human cells
- QUANTIFICATION AND STATISTICAL ANALYSIS
- DATA AND SOFTWARE AVAILABILITY

SUPPLEMENTAL INFORMATION

Supplemental Information includes six figures and three tables and can be found with this article online at http://dx.doi.org/10.1016/j.cell.2016.12.009.

REFERENCES

Abudayyeh, O.O., Gootenberg, J.S., Konermann, S., Joung, J., Slaymaker, I.M., Cox, D.B.T., Shmakov, S., Makarova, K.S., Semenova, E., Minakhin, L., et al. (2016). C2c2 is a single-component programmable RNA-guided RNA-targeting CRISPR effector. Science *353*, aaf5573.

Barrangou, R., and Doudna, J.A. (2016). Applications of CRISPR technologies in research and beyond. Nat. Biotechnol. *34*, 933–941.

Biswas, A., Gagnon, J.N., Brouns, S.J.J., Fineran, P.C., and Brown, C.M. (2013). CRISPRTarget: bioinformatic prediction and analysis of crRNA targets. RNA Biol. *10*, 817–827.

Biswas, A., Staals, R.H.J., Morales, S.E., Fineran, P.C., and Brown, C.M. (2016). CRISPRDetect: a flexible algorithm to define CRISPR arrays. BMC Genomics *17*, 356.

Bondy-Denomy, J., Pawluk, A., Maxwell, K.L., and Davidson, A.R. (2013). Bacteriophage genes that inactivate the CRISPR/Cas bacterial immune system. Nature *493*, 429–432.

Bondy-Denomy, J., Garcia, B., Strum, S., Du, M., Rollins, M.F., Hidalgo-Reyes, Y., Wiedenheft, B., Maxwell, K.L., and Davidson, A.R. (2015). Multiple mechanisms for CRISPR-Cas inhibition by anti-CRISPR proteins. Nature *526*, 136–139.

Brouns, S.J.J., Jore, M.M., Lundgren, M., Westra, E.R., Slijkhuis, R.J.H., Snijders, A.P.L., Dickman, M.J., Makarova, K.S., Koonin, E.V., and van der Oost, J. (2008). Small CRISPR RNAs guide antiviral defense in prokaryotes. Science *321*, 960–964.

Camilli, A., Tilney, L.G., and Portnoy, D.A. (1993). Dual roles of plcA in Listeria monocytogenes pathogenesis. Mol. Microbiol. *8*, 143–157.

Choi, K.-H., Gaynor, J.B., White, K.G., Lopez, C., Bosio, C.M., Karkhoff-Schweizer, R.R., and Schweizer, H.P. (2005). A Tn7-based broad-range bacterial cloning and expression system. Nat. Methods *2*, 443–448.

Cong, L., Ran, F.A., Cox, D., Lin, S., Barretto, R., Habib, N., Hsu, P.D., Wu, X., Jiang, W., Marraffini, L.A., and Zhang, F. (2013). Multiplex genome engineering using CRISPR/Cas systems. Science *339*, 819–823.

Deltcheva, E., Chylinski, K., Sharma, C.M., Gonzales, K., Chao, Y., Pirzada, Z.A., Eckert, M.R., Vogel, J., and Charpentier, E. (2011). CRISPR RNA maturation by trans-encoded small RNA and host factor RNase III. Nature *471*, 602–607.

Di, H., Ye, L., Yan, H., Meng, H., Yamasak, S., and Shi, L. (2014). Comparative analysis of CRISPR loci in different Listeria monocytogenes lineages. Biochem. Biophys. Res. Commun. *454*, 399–403.

East-Seletsky, A., O'Connell, M.R., Knight, S.C., Burstein, D., Cate, J.H.D., Tjian, R., and Doudna, J.A. (2016). Two distinct RNase activities of CRISPR-C2c2 enable guide-RNA processing and RNA detection. Nature *538*, 270–273.

Edgar, R.C. (2004). MUSCLE: multiple sequence alignment with high accuracy and high throughput. Nucleic Acids Res. *32*, 1792–1797.

Edgar, R., and Qimron, U. (2010). The Escherichia coli CRISPR system protects from λ lysogenization, lysogens, and prophage induction. J. Bacteriol. *192*, 6291–6294.

Garneau, J.E., Dupuis, M.-È., Villion, M., Romero, D.A., Barrangou, R., Boyaval, P., Fremaux, C., Horvath, P., Magadán, A.H., and Moineau, S. (2010). The CRISPR/Cas bacterial immune system cleaves bacteriophage and plasmid DNA. Nature *468*, 67–71.

Gilbert, L.A., Larson, M.H., Morsut, L., Liu, Z., Brar, G.A., Torres, S.E., Stern-Ginossar, N., Brandman, O., Whitehead, E.H., Doudna, J.A., et al. (2013). CRISPR-mediated modular RNA-guided regulation of transcription in eukaryotes. Cell *154*, 442–451.

Goldberg, G.W., Jiang, W., Bikard, D., and Marraffini, L.A. (2014). Conditional tolerance of temperate phages via transcription-dependent CRISPR-Cas targeting. Nature *514*, 633–637.

Grissa, I., Vergnaud, G., and Pourcel, C. (2007). CRISPRFinder: a web tool to identify clustered regularly interspaced short palindromic repeats. Nucleic Acids Res. *35*, W52–W57.

Guzman, L.M., Belin, D., Carson, M.J., and Beckwith, J. (1995). Tight regulation, modulation, and high-level expression by vectors containing the arabinose PBAD promoter. J. Bacteriol. *177*, 4121–4130.

Haldimann, A., and Wanner, B.L. (2001). Conditional-replication, integration, excision, and retrieval plasmid-host systems for gene structure-function studies of bacteria. J. Bacteriol. *183*, 6384–6393.

Haurwitz, R.E., Jinek, M., Wiedenheft, B., Zhou, K., and Doudna, J.A. (2010). Sequence- and structure-specific RNA processing by a CRISPR endonuclease. Science *329*, 1355–1358.

Heler, R., Samai, P., Modell, J.W., Weiner, C., Goldberg, G.W., Bikard, D., and Marraffini, L.A. (2015). Cas9 specifies functional viral targets during CRISPR-Cas adaptation. Nature *519*, 199–202.

Jinek, M., Chylinski, K., Fonfara, I., Hauer, M., Doudna, J.A., and Charpentier, E. (2012). A programmable dual-RNA-guided DNA endonuclease in adaptive bacterial immunity. Science *337*, 816–821.

Labrie, S.J., Samson, J.E., and Moineau, S. (2010). Bacteriophage resistance mechanisms. Nat. Rev. Microbiol. *8*, 317–327.

Lauer, P., Chow, M.Y.N., Loessner, M.J., Portnoy, D.A., and Calendar, R. (2002). Construction, characterization, and use of two Listeria monocytogenes site-specific phage integration vectors. J. Bacteriol. *184*, 4177–4186.

Loessner, M.J., and Busse, M. (1990). Bacteriophage typing of Listeria species. Appl. Environ. Microbiol. *56*, 1912–1918.

Makarova, K.S., Wolf, Y.I., Alkhnbashi, O.S., Costa, F., Shah, S.A., Saunders, S.J., Barrangou, R., Brouns, S.J.J., Charpentier, E., Haft, D.H., et al. (2015). An updated evolutionary classification of CRISPR-Cas systems. Nat. Rev. Microbiol. *13*, 722–736.

Mali, P., Yang, L., Esvelt, K.M., Aach, J., Guell, M., DiCarlo, J.E., Norville, J.E., and Church, G.M. (2013). RNA-guided human genome engineering via Cas9. Science *339*, 823–826.

Mandin, P., Repoila, F., Vergassola, M., Geissmann, T., and Cossart, P. (2007). Identification of new noncoding RNAs in Listeria monocytogenes and prediction of mRNA targets. Nucleic Acids Res. *35*, 962–974.

Marraffini, L.A. (2015). CRISPR-Cas immunity in prokaryotes. Nature *526*, 55–61.

Maxwell, K.L., Garcia, B., Bondy-Denomy, J., Bona, D., Hidalgo-Reyes, Y., and Davidson, A.R. (2016). The solution structure of an anti-CRISPR protein. Nat. Commun. *7*, 13134.

Mojica, F.J.M., Díez-Villaseñor, C., García-Martínez, J., and Soria, E. (2005). Intervening sequences of regularly spaced prokaryotic repeats derive from foreign genetic elements. J. Mol. Evol. *60*, 174–182.

Nuñez, J.K., Kranzusch, P.J., Noeske, J., Wright, A.V., Davies, C.W., and Doudna, J.A. (2014). Cas1-Cas2 complex formation mediates spacer acquisition during CRISPR-Cas adaptive immunity. Nat. Struct. Mol. Biol. *21*, 528–534.

Park, S.F., and Stewart, G.S. (1990). High-efficiency transformation of Listeria monocytogenes by electroporation of penicillin-treated cells. Gene *94*, 129–132.

Pawluk, A., Bondy-Denomy, J., Cheung, V.H.W., Maxwell, K.L., and Davidson, A.R. (2014). A new group of phage anti-CRISPR genes inhibits the type I-E CRISPR-Cas system of Pseudomonas aeruginosa. MBio *5*, e00896, e00896–e14.

Pawluk, A., Staals, R.H.J., Taylor, C., Watson, B.N.J., Saha, S., Fineran, P.C., Maxwell, K.L., and Davidson, A.R. (2016). Inactivation of CRISPR-Cas systems by anti-CRISPR proteins in diverse bacterial species. Nat. Microbiol. *1*, 16085.

Qi, L.S., Larson, M.H., Gilbert, L.A., Doudna, J.A., Weissman, J.S., Arkin, A.P., and Lim, W.A. (2013). Repurposing CRISPR as an RNA-guided platform for sequence-specific control of gene expression. Cell *152*, 1173–1183.

Ran, F.A., Cong, L., Yan, W.X., Scott, D.A., Gootenberg, J.S., Kriz, A.J., Zetsche, B., Shalem, O., Wu, X., Makarova, K.S., et al. (2015). In vivo genome editing using Staphylococcus aureus Cas9. Nature *520*, 186–191.

Samai, P., Pyenson, N., Jiang, W., Goldberg, G.W., Hatoum-Aslan, A., and Marraffini, L.A. (2015). Co-transcriptional DNA and RNA cleavage during Type III CRISPR-Cas immunity. Cell *161*, 1164–1174.

Samson, J.E., Magadán, A.H., Sabri, M., and Moineau, S. (2013). Revenge of the phages: defeating bacterial defences. Nat. Rev. Microbiol. *11*, 675–687.

Sesto, N., Touchon, M., Andrade, J.M., Kondo, J., Rocha, E.P.C., Arraiano, C.M., Archambaud, C., Westhof, É., Romby, P., and Cossart, P. (2014). A PNPase dependent CRISPR system in Listeria. PLoS Genet. *10*, e1004065.

Söding, J., Biegert, A., and Lupas, A.N. (2005). The HHpred interactive server for protein homology detection and structure prediction. Nucleic Acids Res. *33*, W244–W248.

Tamura, K., Stecher, G., Peterson, D., Filipski, A., and Kumar, S. (2013). MEGA6: Molecular Evolutionary Genetics Analysis version 6.0. Mol. Biol. Evol. *30*, 2725–2729.

Typas, A., Nichols, R.J., Siegele, D.A., Shales, M., Collins, S.R., Lim, B., Braberg, H., Yamamoto, N., Takeuchi, R., Wanner, B.L., et al. (2008). High-throughput, quantitative analyses of genetic interactions in E. coli. Nat. Methods *5*, 781–787.

Wang, X., Yao, D., Xu, J.-G., Li, A.-R., Xu, J., Fu, P., Zhou, Y., and Zhu, Y. (2016). Structural basis of Cas3 inhibition by the bacteriophage protein AcrF3. Nat. Struct. Mol. Biol. *23*, 868–870.

Wright, A.V., Nuñez, J.K., and Doudna, J.A. (2016). Biology and applications of CRISPR systems: harnessing nature's toolbox for genome engineering. Cell *164*, 29–44.

Yosef, I., Goren, M.G., and Qimron, U. (2012). Proteins and DNA elements essential for the CRISPR adaptation process in Escherichia coli. Nucleic Acids Res. *40*, 5569–5576.

Zemansky, J., Kline, B.C., Woodward, J.J., Leber, J.H., Marquis, H., and Portnoy, D.A. (2009). Development of a mariner-based transposon and identification of Listeria monocytogenes determinants, including the peptidyl-prolyl isomerase PrsA2, that contribute to its hemolytic phenotype. J. Bacteriol. *191*, 3950–3964.

Zetsche, B., Gootenberg, J.S., Abudayyeh, O.O., Slaymaker, I.M., Makarova, K.S., Essletzbichler, P., Volz, S.E., Joung, J., van der Oost, J., Regev, A., et al. (2015). Cpf1 is a single RNA-guided endonuclease of a class 2 CRISPR-Cas system. Cell *163*, 759–771.

Cell

STAR★METHODS

KEY RESOURCES TABLE

REAGENT or RESOURCE	SOURCE	IDENTIFIER
Experimental Models: Cell Lines		
HEK293T	ATCC	N/A
Experimental Models: Organisms/Strains		
Listeria monocytogenes 10403s	Laboratory of Anna Bakardjiev	ncbi.nlm.nih.gov/Taxonomy/Browser/wwwtax.cgi?mode = Info&id = 393133&lvl = 3&lin = f&keep = 1&srchmode = 1&unlock
Listeria monocytogenes 10403s derivatives	This paper	See Table S2
Listeria monocytogenes J0161	Laboratory of Martin Wiedmann	ncbi.nlm.nih.gov/Taxonomy/Browser/wwwtax.cgi?id = 393130
Listeria monocytogenes SLCC2482	Ariane Pietzka	ncbi.nlm.nih.gov/Taxonomy/Browser/wwwtax.cgi?id = 863767
Listeria monocytogenes SLCC2540	Ariane Pietzka	ncbi.nlm.nih.gov/Taxonomy/Browser/wwwtax.cgi?id = 879089
Escherichia coli BW25113 derivatives	This paper	See Table S2
Recombinant DNA		
pBAD24	Laboratory of Carol Gross	ncbi.nlm.nih.gov/nuccore/X81837.1
pBAD24-derivative plasmids	This paper	See Table S2
pdCas9-bacteria	Addgene	addgene.org/vector-database/44249/
pLVX-TetOne-Puro	Clontech	clontech.com/US/Products/Inducible_Systems/TetSystems_Product_Overview/Tet-One_Overview
pMD2.G	Addgene	addgene.org/12259/
pX330	Addgene	addgene.org/vector-database/42230/
pcDNA3.1(+)	Addgene	addgene.org/vector-database/2093/
pKSV7	Laboratory of Anna Bakardjiev	addgene.org/26686/
pKSV7-derivative plasmids	This paper	See Table S2
pPL2oexL	Laboratory of Daniel Portnoy	See Figure S6
pPL2oexL-derivative plasmids	This paper	See Table S2
Sequence-Based Reagents		
GeneBlocks for HEK293T expression of phage proteins	IDT	See Table S3
Software and Algorithms		
Prism 5	GraphPad	graphpad.com/scientific-software/prism/
CRISPRfinder	I2BC	crispr.i2bc.paris-saclay.fr/Server/
CRISPRDetect	Univsersity of Otago	brownlabtools.otago.ac.nz/CRISPRDetect/predict_crispr_array.html
CRISPRtarget	Univsersity of Otago	bioanalysis.otago.ac.nz/CRISPRTarget/crispr_analysis.html
illustrator	Adobe	adobe.com/Illustrator
MEGA6	MEGA	megasoftware.net/
Image Lab 5.2.1	BioRad	bio-rad.com/en-cn/product/image-lab-software
FlowJo	FlowJo LLC	flowjo.com/

CONTACT FOR REAGENT AND RESOURCE SHARING

Please direct any requests for further information or reagents to the Lead Contact, Joseph Bondy-Denomy (joseph.bondy-denomy@ucsf.edu), Department of Microbiology and Immunology, University of California, San Francisco.

EXPERIMENTAL MODEL AND SUBJECT DETAILS

Microbes
Listeria monocytogenes strains were cultured on Brain-Heart Infusion (BHI) medium. *Escherichia coli* strains were cultured on LB medium.

Cell lines
Human Embryonic Kidney 293 plus T cell antigen (HEK293T, CRL-3216, ATCC) cells were cultured in Dulbecco's Modified Eagle's Medium (DMEM) supplemented with 10% fetal bovine serum (FBS, Atlanta Biologicals) and 50 μg/mL penicillin/streptomycin (P/S, UCSF CCF).

METHOD DETAILS

Assay of CRISPR-Cas9 in L. monocytogenes
Plasmid-transformation assay of CRISPR-Cas9
Targeted (pT; pNT for J0161; pRAU31) and non-targeted (pNT; pT$_{J0161}$; pRAU29) plasmids for *L. monocytogenes* 10403s were constructed by ligating annealed primer pairs into the HindIII and BamHI sites of pKSV7. See Table S3 for plasmid-insert sequences. *L. monocytogenes* strains were transformed with 0.5-1.0 μg pT or pNT by electroporation. Electrocompetent cells were prepared and transformed as described (Park and Stewart, 1990; Zemansky et al., 2009). Transformations were diluted 10-fold into BHI and recovered for two hours, shaking at 30°C. Recovered cultures were plated on BHI with 1.5% agar and 7.5 μg/ml chloramphenicol to select for pT or pNT. For pPL2oexL integrants, tetracycline selection (2 μg/ml) was maintained throughout the procedure, with exception to recovery cultures, which were performed without selection. Whereas plates that contained only chloramphenicol were incubated at 30°C for 36-40 hr prior to imaging, plates that also contained tetracycline were incubated at 30°C for 64-72 hr. Plate images were collected using the Gel Doc EZ Gel Documentation System (BioRad) and Image Lab (BioRad) software.

Construction of pPL2oexL-integrants in L. monocytogenes 10403s
The pPL2oexL plasmid for constitutive chromosomal expression of genes in *L. monocytogenes* was derived from pPL2 (Lauer et al., 2002) (see Figure S6). Individual genes or phage fragments were PCR-amplified from genomic DNA and cloned into pPL2oexL by Gibson Assembly. pPL2oexL-derivative plasmids were electroporated into nonlysogenic 10403s, using a procedure like that which was employed for the plasmid-transformation assay of CRISPR-Cas9 (see text under previous heading). Transformations were recovered for two hours, shaking at 37°C and were plated on BHI-agar with 2 μg/ml tetracycline. Colonies emerged after 36-48 hr incubating at 37°C, and were re-streaked once on the same selective medium to ensure genotypic homogeneity.

Construction of a 10403s::ϕJ0161a lysogen
Phage was induced from *L. monocytogenes* strain J0161 by exposure to ultraviolet radiation as described previously (Loessner and Busse, 1990). 10403s::ϕJ0161a lysogens were isolated from plaques that resulted from spotting amplified J0161 phage stock on a lawn of nonlysogenic 10403s (suspended in BHI with 0.7% agar and 2.5 mM CaCl$_2$). Plaques emerged after 16 hr incubation at 30°C. Lysogeny was confirmed by PCR, as described (Lauer et al., 2002).

Construction of markerless chromosomal deletion strains
Markerless deletions of *cas9* and *acrIIA1-2* were constructed by allelic exchange in nonlysogenic 10403s and 10403s::ϕJ0161a, respectively. Up- and down-stream (700-1000 base pairs) regions flanking the genes to be deleted were fused by overlap-extension PCR and ligated into pKSV7. The $\Delta cas9$ genotype was inserted between the HindIII and BamHI restriction sites, whereas the $\Delta acrA1-2$ genotype was inserted between the SacI and BamHI restriction sites. Knockout vectors were transformed by electroporation. Subsequent manipulations were performed as previously reported (Camilli et al., 1993).

Bioinformatic analyses
Identification of self-targeting CRISPR-Cas systems
L. monocytogenes genome sequences were downloaded from NCBI. Type-IIA CRISPR arrays were identified within individual genomes using CRISPRfinder (Grissa et al., 2007) or CRISPRDetect (Biswas et al., 2016) web utilities. See Figure S1B for a representative *L. monocytogenes* type II-A CRISPR array. Self-targeting CRISPR-Cas systems were identified using the CRISPRtarget web utility (Biswas et al., 2013) by searching individual *L. monocytogenes* genomes with their own CRISPR arrays. Bona fide self-targeting events were defined as perfect matches lacking spacer-protospacer mutations in the PAM-proximal region (20 bp), concurrent with a cognate PAM sequence (5′-NGG-3′). See Table S1 for a list of self-targeting strains.

Cell

Phylogenetic reconstruction of AcrIIA protein families

AcrIIA2- (AEO04363.1), AcrIIA3- (CBY03209.1) and AcrIIA4- (AEO04689.1) homologous protein sequences were acquired by BLASTp searches of all the non-redundant protein sequence database of NCBI on November 5, 2016. Full-length (> 78% query coverage) sequences of high homology (E value < 1e-04) were downloaded and aligned using Muscle (Edgar, 2004) in MEGA6 (Tamura et al., 2013). Phylogenetic reconstructions of each protein family were performed in MEGA6 using the neighbor-joining method with the Poisson model for amino acid substitution, uniform rates among sites and pairwise deletion of gaps. Reconstructions were tested using the bootstrap method (1000 replications). Reconstruction images were then edited for clarity in Illustrator (Adobe). AcrIIA1- (AEO04364.1) homologous protein sequences were acquired by four iterations of psiBLASTp searches of the non-redundant protein sequence database of NCBI on October 26, 2016. The position-specific scoring matrix (PSSM) was enchriched with all full-length (> 80%) protein sequences. Sequences were downloaded, aligned, and reconstructed using the same methodology that was employed for the analysis of AcrIIA2, 3 and 4 (see above). However, in the case of AcrIIA1, sequences with large insertions (> 30 amino acids) were removed from the sequence alignments, prior to phylogenetic reconstruction.

Analysis of gene-conservation patterns

The conservation of *acrIIA1*, *acrIIA2*, *acrIIA3*, *acrIIA4* and *cas9* were cataloged in reference to a control gene (cysteinyl-tRNA synthetase) that occurs once in all *L. monocytogenes* genomes. BLASTp searches were performed to acquire lists of genome-specific accession numbers for encoded proteins. These were used as surrogates for genes to assess conservation. Lists were compiled into a single table and sorted so that individual rows of data included accession numbers for all proteins of interest encoded within a single genome.

Inhibition of Spy-CRISPRi in *E. coli*

Reporter strain construction

Our *E. coli* Spy-CRISPRi reporter system uses integrated components of the previously reported CRISPRi system (Qi et al., 2013) with minor modifications. The promoter for *mrfp* was modified in the entry vector by changing the promoter from PLlacO-1 to a minimal synthetic promoter (BBa_J23119) (http://parts.igem.org/Main_Page), PCR amplified, and integrated into BW25113 at *nfsA* by recombineering as described. The *mrfp*-targeting sgRNA was cloned into the site-specific integrating plasmid pCAH63 under control of PLlacO-1 to generate pCs550-r, and integrated at lambda att using the helper plasmid pINT-ts (Haldimann and Wanner, 2001), selecting for chloramphenicol resistance. Conjugation was used to move a chromosomal *dcas9* cassette into recipient strains harboring *mrfp*, sgRNA or both. A "pseudo-Hfr" strain isogenic with BW25113, carries the transfer region from F and a spectinomycin marker integrated downstream of *rhaM* (4086kb) (Typas et al., 2008). A "pseudo-Hfr" *dcas9* donor strain was constructed by integrating *dcas9* and a gentamycin resistance marker at the Tn7 att site (Choi et al., 2005), adjacent to the origin of transfer. *dcas9* was cloned from pdCas9-bacteria (Addgene #44249) under control of BBa_J23105 (http://parts.igem.org/Main_Page). Putative Cas9 inhibitor proteins were cloned into pBAD24 (Guzman et al., 1995) by Gibson Assembly (NEB) and transformed into the *Spy*-CRISPRi strains by electroporation.

Flow cytometry

Strains were grown overnight in LB with arabinose in deep 96-well plates, and then back-diluted 1:400 into fresh LB with arabinose (to maintain expression of the inhibitor) and IPTG (to induce expression of the sgRNA). After 2.5hr growth (OD~0.4) cultures were fixed using 1.5% final formaldehyde and quenched with glycine, and then diluted 1:30 into phosphate buffered saline. Red fluorescence levels were measured using an LSRII flow cytometer (BD Biosciences) using the yellow/green laser (561 nm) and the PE-Texas Red® detector (610/20 nm). Data for at least 20,000 cells were collected, and median fluorescence values were extracted using FlowJo (FlowJo, LLC). Error bars represent the standard deviation from 3 or more biological replicates. Data from representative samples were plotted as histograms using FlowJo.

Inhibition of Cas9 cleavage in human cells

An eGFP-targeting crRNA was ordered as complementary single-stranded DNA oligos (IDT) and cloned into BbsI linearized pX330 (Addgene, Zhang lab) to generate a single vector expressing S. pyrogenes Cas9-NLS and an eGFP-targeting CRISPR cassette. One candidate (orf) and three validated (acr) acrIIA genes were codon-optimized for human cell expression, synthesized in vitro (IDT, GeneBlock), and cloned into BamHI/EcoRI linearized pcDNA3.1(+) by Gibson assembly. Similarly, the gene encoding enhanced Green Fluorescent Protein (eGFP) was synthesized and cloned into BamHI/EcoRI linearized pLVX-TetOne-Puro (Clontech). Doxycycline-inducible eGFP lentivirus was produced in Human Embryonic Kidney (HEK)293T cells (ATCC) by cotransfection (polyJet, SignaGen) with Gag-Pol packaging construct and VSV-G envelope (pMD2.G, Addgene). Lentiviruses were precipitated from the cellular supernatant at 4°C by incubation in a final concentration of 8.5% Poly(ethylene glycol) average Mn 6000 (PEG-6000) and 0.3M NaCl for 4 hr. Viruses were concentrated at 3500 RPM for 20 min in a spinning bucket rotor, suspended in 1 mL 1xPBS, and preserved at −80. One-thousandth viral preparation by volume was used to transduce 250,000 HEK293T cells and successful integrants purified by selection in 1 μg/mL puromycin for 48 hr.

Polyclonal HEK293T cells with a chromosomally integrated, inducible eGFP cassette were expanded, plated, and transfected with the eGFP-targeting CRISPR construct and each of the bacteriophage genes at different ratios in triplicate (Trans-IT, Mirus). An empty vector was used to equalize the total mass of transfected plasmid across each sample. 36 hr after transfection, cells were treated with 2 μg/mL doxycycline to induce eGFP expression. 12 hr later, cells were suspended by incubation in PBS-EDTA, fixed in 1%

formaldehyde PBS, and percent eGFP-positive cells monitored by flow cytometry (FACSCalibur, Gladstone Flow Cytometry Core). Data were normalized to no sgRNA controls and presented as the average percent eGFP-positive cells ± standard deviation.

QUANTIFICATION AND STATISTICAL ANALYSIS

All experiments were conducted with at least three biological replicates (N > = 3). Statistical parameters are reported in the Figures and the Figure Legends. Additional statistical tests were not performed.

DATA AND SOFTWARE AVAILABILITY

The accession numbers, locus tags, and coding sequences for individual genes tested for CRISPR-Cas9 inhibition activity are disclosed in Figure S3. Additional accession numbers for AcrIIA homologs are reported in Table S1.

Figure S1. Self-Targeting by CRISPR-Cas9 in *Listeria monocytogenes* J0161 Is Not Associated with Loss-of-Function Mutations, Related to Figure 1

(A) Comparison of type II-A CRISPR-*cas* loci from *Streptococcus pyogenes* SF370 (*Spy_SF370*), *Listeria monocytogenes* 10403s (*Lmo_10403s*), *Listeria monocytogenes* J0161 (*Lmo_J0161*) and *Listeria innocua* (*Lin_Clip11262*). Percent identity between Cas9 protein sequences is shown.

(B) The CRISPR array of self-targeting strain *Lmo* J0161. A type II-A CRISPR array, predicted by the CRISPRDetect web utility is shown. The self-targeting spacer (number 16) is boxed. In bold, are the RNA-coding nucleotides responsible for target recognition.

(C) Alignment of tracrRNA loci.

(D) Alignment of CRISPR loci.
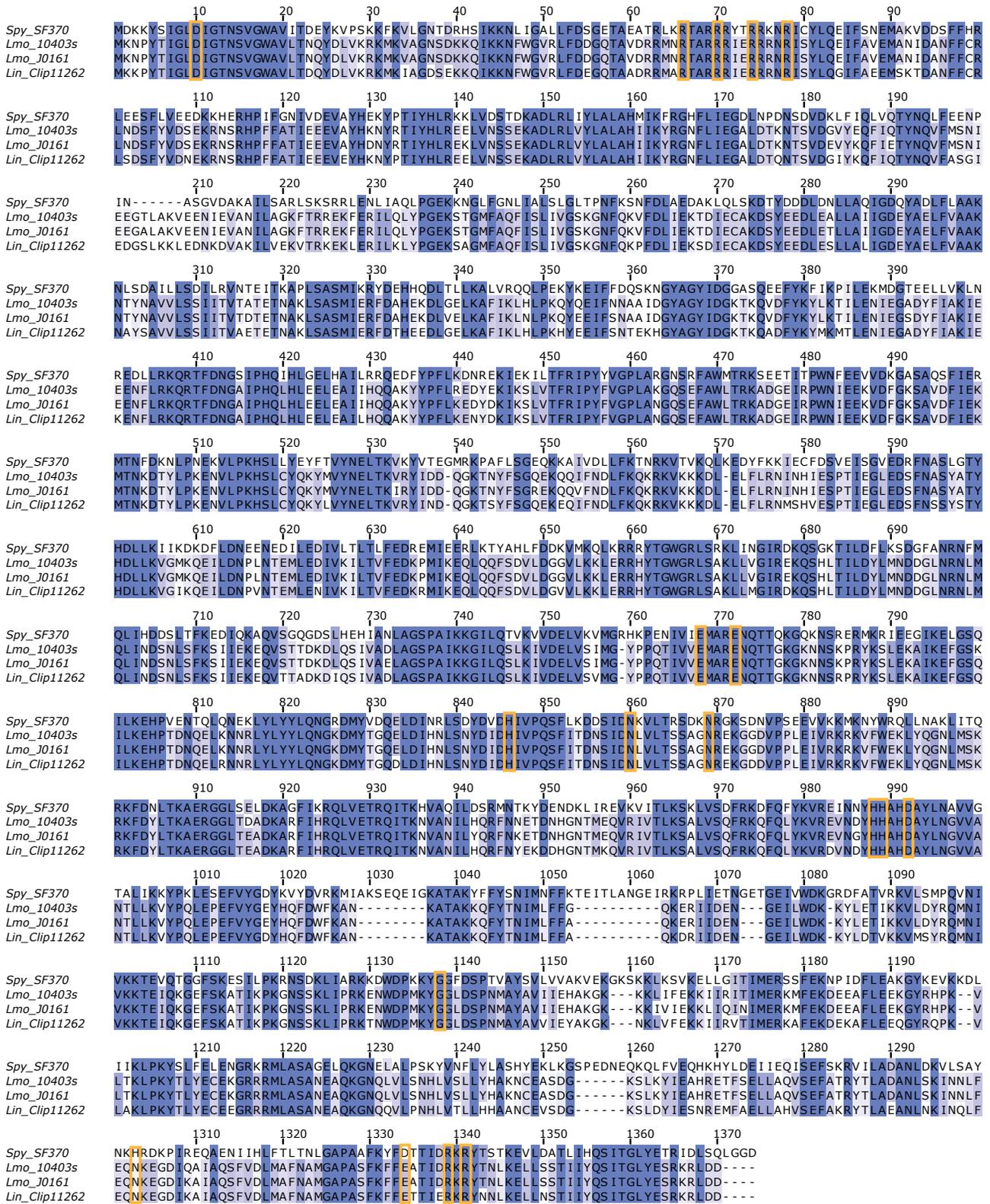
Figure S2. Cas9 Protein Sequence Alignment, Related to Figures 1 and S1

Alignment of Cas9 protein sequences. Residues with essential chemical functionalities are boxed.
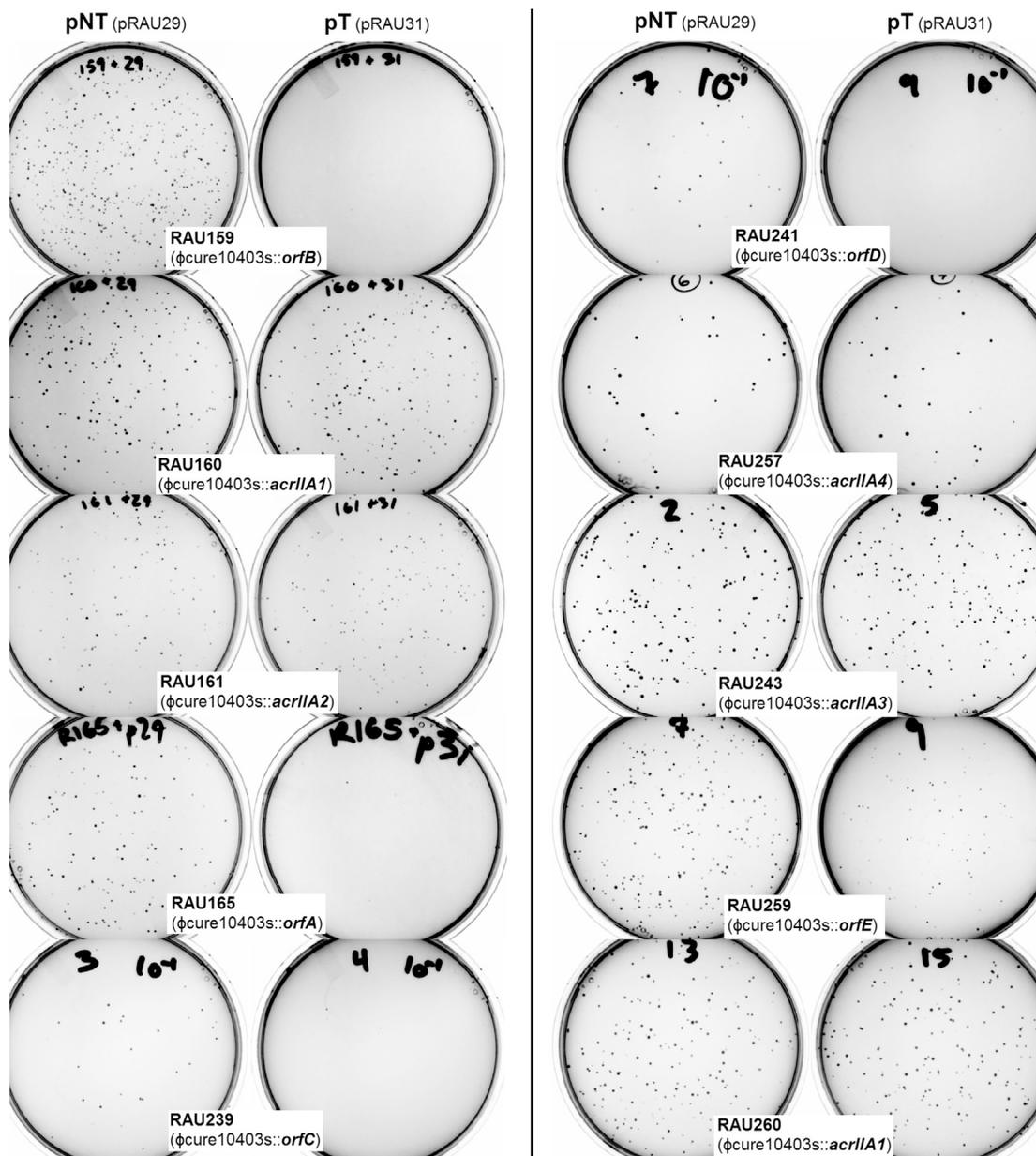
Figure S3. Individual Genes that Were Screened for CRISPR-Cas9 Inhibition Activity in *L. monocytogenes* 10403s, Related to Figures 3B, 3C, and 4A

Representative plates depicting colonies after transformation and selection for targeted (pT; pRAU31) or non-targeted (pNT; pRAU29) plasmids. Given names, and strain numbers are provided. See Table S2 for additional information pertinent to plasmid and strain design and nomenclature. See Table S3 for gene sequences.
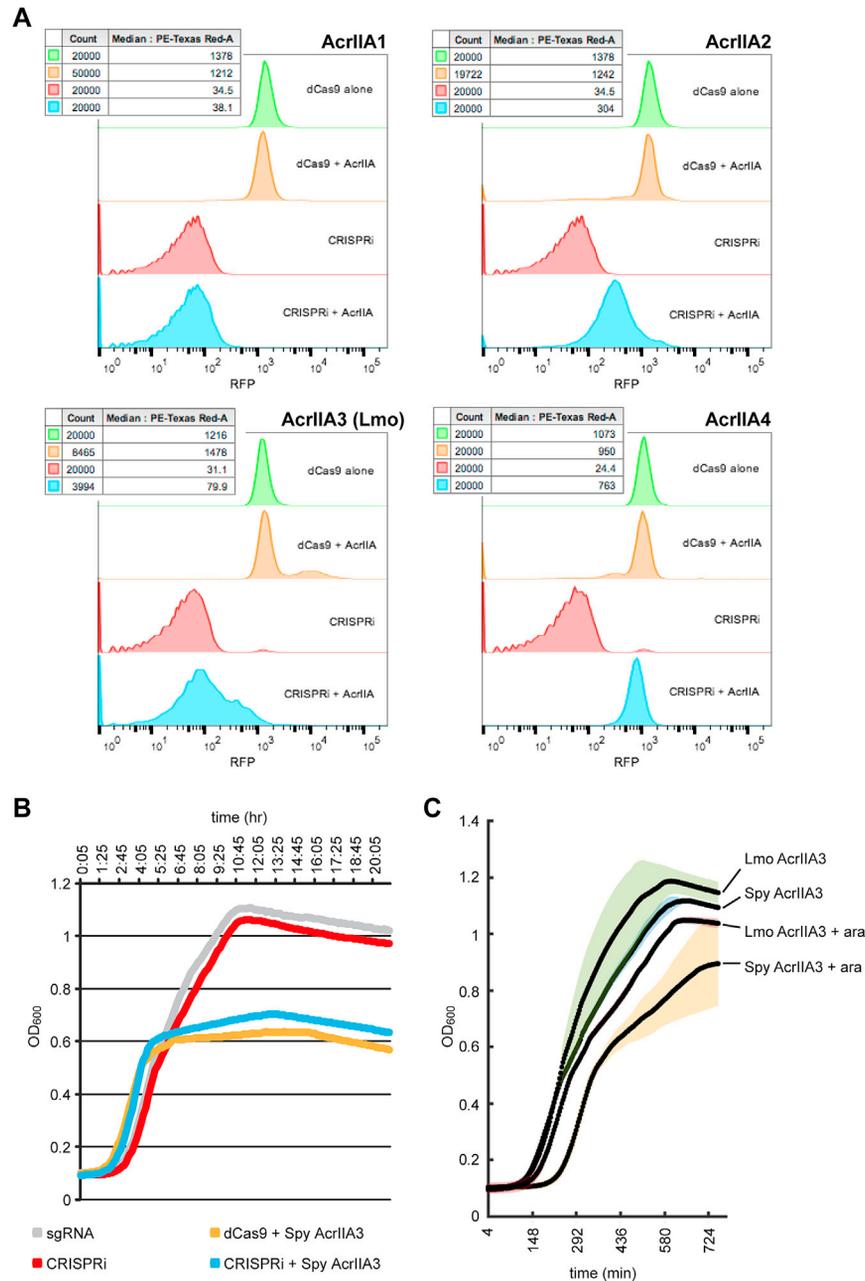
Figure S4. Toxicity of an AcrIIA3 Homolog from *S. pyogenes* in *E. coli*, Related to Figure 6B

(A) Distribution of single-cell RFP fluorescence values for *E. coli* CRISPRi reporter strains with and without expression of AcrIIA proteins. Expression of AcrIIA proteins leads to unimodal shift in population fluorescence toward the sgRNA (no CRISPRi knockdown) state, indicating a uniform disruption of CRISPRi activity. Strains were grown for 2.5hr in the presence of IPTG to induce CRISPRi, with or without expression of the AcrIIA inhibitor.

(B) Expression of Spy AcrIIA3 is toxic in *E. coli*. In the presence of IPTG (CRISPRi induction) and arabinose (AcrIIA3 induction), Spy AcrIIA3 is toxic in the presence or absence of sgRNA, indicating that its toxicity is independent of CRISPRi activity.

(C) Expression of either acrIIA3 ortholog is toxic in *E. coli*. Indicated strains express all components for CRISPRi and were grown in microtiter plates with or without 0.0005% arabinose (AcrIIA3 expression induction) and 1mM IPTG (CRISPRi induction), and optical density was monitored every 4 min. Plots depict the mean of three biological replicates ± SD.
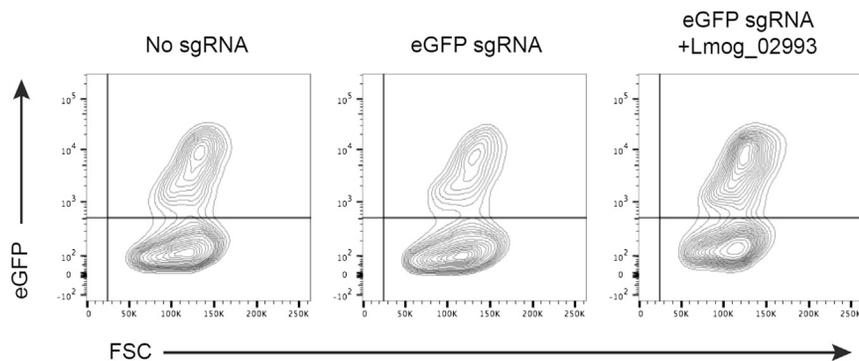
Figure S5. Inhibition of *S. pyogenes* Cas9 by AcrIIA4 in Human Cells, Related to Figure 6D

HEK293T cells were analyzed for eGFP expression 12 hr post-induction by flow cytometry. Representative flow plots from one biological replicate are depicted for cells that received Cas9 with no guide RNA (No sgRNA), Cas9 with an eGFP-targeting guide RNA (eGFP sgRNA), and Cas9 with an eGFP-targeting guide RNA and an independent AcrII4 expression vector (eGFP sgRNA + AcrII4). Forward scatter is depicted on the horizontal axis and eGFP fluorescence on the vertical axis. Vertical gating was set with cells that did not receive induction with doxycycline.

20160420 GA177 pPL2oexL FLAG
8986 bp
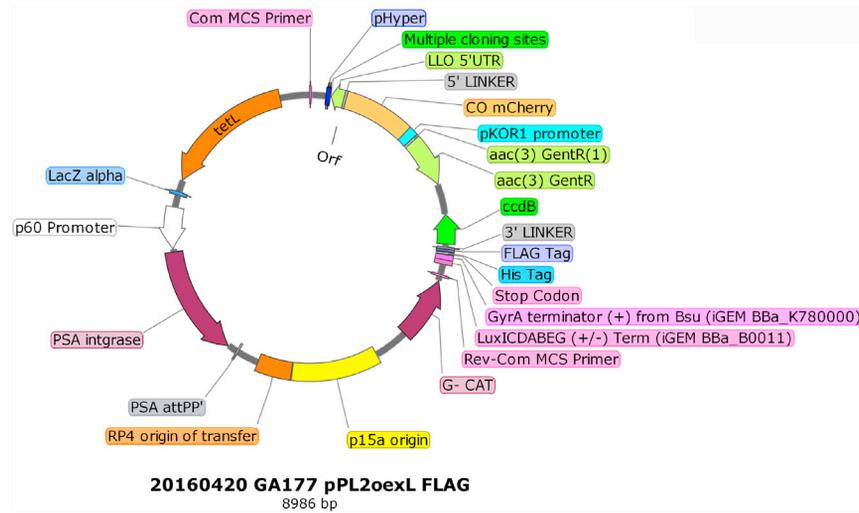
Figure S6. Vector Map File for pPL2oexL, Related to STAR Methods
Genes and phage fragments to be tested for CRISPR-Cas9 inhibition in *L. monocytogenes* 10403s were cloned into pPL2oexL between pHyper and the FLAG tag. Native stop codons were included in pPL2oexL derivatives.